Journal of CO2 Utilization 62 (2022) 102105

Contents lists available at ScienceDirect

Journal of CO2 Utilization

journal homepage: www.elsevier.com/locate/jcou

Supercritical carbon dioxide enhanced natural gas recovery from kerogen micropores

Kai Bin Yu [a], Geoffrey M. Bowers [b], A. Ozgur Yazaydin [a,*]

[a] Department of Chemical Engineering, University College London, London WC1E 7JE, United Kingdom
[b] Department of Chemistry and Biochemistry, St. Mary's College of Maryland, St. Mary's City, MD 20686, USA

ARTICLE INFO

Keywords:
Molecular simulation
Carbon sequestration
Adsorption kinetics
Hydraulic fracturing
Enhanced gas recovery

ABSTRACT

As the global energy demand increases, a sustainable and environmentally friendly methane (CH_4) extraction technique must be developed to assist in the transition off of fossil fuels. In recent years, supercritical carbon dioxide (CO_2) has been poised as a candidate for enhanced gas recovery (EGR) from CH_4-rich source rocks, potentially with the reservoir serving as a carbon sink for CO_2. However, the underlying molecular-scale mechanisms of CO_2-EGR processes are still poorly understood. Using constant chemical potential molecular dynamics (CμMD), this study investigates the CH_4 recovery process via supercritical CO_2 injection into immature (Type I-A) and overmature (Type II-D) kerogens in real-time and at reservoir conditions (365 K and 275 bar). A pseudo-second order (PSO) rate law was used to quantify the adsorption and desorption kinetics of CO_2 and CH_4. The kinetics of simultaneous adsorption/desorption are rapid in immature kerogen due to better connected pore volume facilitating fluid diffusion, whereas in overmature kerogen, the structural heterogeneity hinders fluid diffusion. Estimated second order kinetic rate coefficients reveal that CO_2 adsorption and CH_4 desorption in Type I-A are about two times and an order of magnitude faster, respectively, compared to those of in Type II-D. Furthermore, overmature Type II-D kerogen contains inaccessible micropores which prevent full recovery of CH_4. For every CH_4 molecule replaced, at least two and six CO_2 molecules are adsorbed in Type-II-D and Type I-A kerogens, respectively. Overall, this study shows that CO_2 injection can achieve 90 % and 65 % CH_4 recovery in Type I-A and Type II-D kerogens, respectively.

1. Introduction

A net-zero emission future is vital in controlling global heating and preventing adverse climate disasters to come. Despite the increasing demand for renewable energy, it is projected that fossil fuels will remain the largest share in the global energy portfolio for many years. Of all the fossil fuels, natural gas consisting of mainly methane (CH_4) is considered the cleanest, generating less air pollution and greenhouse gas emissions when burnt in the same quantity as coal and petroleum. In recent years, significant effort has gone into exploring unconventional sources of natural gas such as shale gas, tight gas, and coalbed methane (CBM) [1,2]. To date, a significant amount of source rock reserves have been discovered, of which 647.95 trillion m^3 of shale gas are technically recoverable [3], and successful commercial exploitation could help to alleviate a potential energy crisis. The combination of both horizontal drilling and hydraulic fracturing techniques has accelerated the production of shale gas and coal seam gas, however, unconventional gas production still faces a low recovery rate of 20 % or less and CH_4 emissions are at least 30 % higher than that of conventional natural gas reserves [4–7]. To reach these yields, chemical additives are introduced into hydraulic fracturing fluids in the amount of 0.05–1.5 wt. % of the total hydraulic fracturing fluid. Though these are seemingly small quantities, a substantial amount of additives are used over the full lifetime of a well (150–600 m^3). There is very little published data regarding the composition or identity of the chemical additives used owing to trade secret protection. The US EPA has identified over 1000 chemical substances that have been used as chemical additives between 2005 and 2013 [8]. The FracFocus database [9] indicates that chemical additives that may eventually break down to perfluoroalkyl and polyfluoroalkyl substances (PFAS), also known as "forever chemicals", have been used commercially since 2011. The impacts of these additives on human health and biodiversity in the environment remain largely unknown, through preliminary studies suggest those additives can cause developmental and reproductive harm to mammals [10,11]. In order to

* Corresponding author.
E-mail address: ozgur.yazaydin@ucl.ac.uk (A.O. Yazaydin).

https://doi.org/10.1016/j.jcou.2022.102105
Received 13 April 2022; Received in revised form 17 May 2022; Accepted 16 June 2022
Available online 20 June 2022
2212-9820/© 2022 The Author(s). Published by Elsevier Ltd. This is an open access article under the CC BY license (http://creativecommons.org/licenses/by/4.0/).

achieve a long-term safe and sustainable production whilst achieving global climate targets over the coming decades, i.e., net-zero emissions, it is vital to eliminate or replace the toxic chemical additives used in hydrofracking fluids.

One method that could eliminate the use of water-based fluids and the additives they require is the use of supercritical CO_2 as a means of enhanced gas recovery (EGR) that may or may not be coupled with geological CO_2 sequestration (GCS) [12–16]. Techniques such as CO_2 injection [17–20] and liquid CO_2 fracturing [21] can be used to deliver CO_2 into unconventional reservoirs. The latter has shown great promise with an increased extraction efficiency by up to 50 %, whereas traditional hydraulic fracturing extraction is often hindered by the formation of ordered water in the micro and mesopores, causing low gas productivity [22–24]. Thus far, CO_2 injection-based EGR has yet to be developed to its fullest potential, and doing so requires that we learn more about the molecular-scale behaviours that influence gas recovery and the gas recovery mechanisms; a vital step towards achieving economic viability of a CO_2-based process [25].

Methane exists in various dynamic fluid states within the shale micropores, i.e., free (in fractures and pores), adsorbed (surfaces of shale matrix), and dissolved (absorbed within organic matter like kerogen) states [26–28]. It has been established that the adsorbed gas dominates the total gas in place (GIP) – up to 85 % of the GIP is adsorbed CH_4 [29, 30]. Adsorbed gas is located mainly in the organic parts of the shale matrix that are dominated by waxy substances known as kerogen [31–36]. Kerogens are derived from geological transformations of buried marine microorganisms exposed to elevated temperatures and pressures within the earth. As a result, kerogen composition varies with the age and T/P history of the source rock, with kerogens becoming more carbon-rich, lower molecular mass, and increasingly dense with increasing T, P, and time. However, in general kerogens are composed of large hydrocarbon backbones functionalized with some oxygen-bearing groups with the molecular units packed together in a disordered manner, leading to a diversity of complex and heterogeneous microporous and mesoporous structures.

Several experimental and theoretical studies have demonstrated that kerogen or proxies of it (e.g., carbon nanotubes (CNTs), graphite, and etc.) preferentially adsorb CO_2 over CH_4 [37–51], though the mechanisms that underpin gas recovery are not fully understood. Probing the phase behaviour of fluids in confined kerogen micropores poses a challenge for experimental studies, as do the length and time scale involved for time-dependent dynamic processes such as competitive adsorption and gas displacement at the nanoscale. Molecular simulations have become one of the most popular methods to provide molecular-scale insight into fluid–kerogen interactions, complementing experimental observations [39,52]. In recent years, atomistic simulation techniques such as grand canonical Monte Carlo (GCMC) [53–55] and molecular dynamics (MD) [56–60] have been used to study fluid adsorption and diffusion/transport in model shale matrices. The hybrid GCMC/MD simulations [61–63] has advanced our understanding of adsorption in shale by taking into account sorption-induced strain. A great deal of literature has been reviewed in our recent study [64] examining various packing procedures to generate kerogen matrices of different maturity levels and the effects the packing procedure has on the CH_4 diffusion behaviour. In the remainder of this introduction, we will focus on recent progress made modelling CO_2-EGR in kerogen systems.

In 2017, Sun et al. [40] offered molecular insights into CH_4 displacement by CO_2 injection in a 21 Å wide slit-shaped nanopore of mature kerogen developed by Collell et al. [65]. They reported higher CO_2 adsorption capacities compared to CH_4 in kerogen. They also show that the fluid diffusion rate is slowest for pores within the kerogen matrix < internal surface of slit pore < central pore region due the varying degree of fluid interactions with the kerogen pore surfaces. CH_4 and CO_2 adsorption energies on the surface of the kerogen fragments showed that CH_4 has a weaker interaction with the kerogen surfaces compared to that of CO_2. In addition, the former has been shown to adsorb relatively uniformly across the kerogen surface, whereas the latter adsorbs more strongly to hydroxyl groups. Through NVT MD simulations at varying bulk CO_2 pressures between 6 and 20 MPa, they demonstrated that the higher the bulk pressure, the higher the CH_4 recovery rate, reporting a maximum recovery of 84 % at 20 MPa. Importantly, their result shows that a small amount of CH_4 adsorbed within the matrix remained unrecoverable. Through simulated annealing, Pathak et al. [58] showed the sorption induced volumetric strain of a kerogen matrix made up of 15 Type II-C kerogen molecules when exposed to a total of 750 molecules of CH_4 and/or CO_2 at 400 K and 300 atm. They found that the diffusion coefficient of CH_4 is an order of magnitude higher than that of CO_2 and that CH_4 imbibition resulted in swelling of the kerogen matrices. However, replacing the CH_4 with CO_2 led to shrinkage of the kerogen matrix volume of 75 % or higher. They suggested that a greater volume of CO_2 must be injected than the GIP to ensure the kerogen matrix does not deform. More recently, Babatunde et al. [66] modelled CH_4/CO_2 adsorption in shale through GCMC simulations using a slit-shaped nanocomposite made of 60 % clay minerals (montmorillonite and illite), 10 % Type II-D kerogen and 30 % quartz. The proposed shale model was found to have a superior adsorption capacity and surface area compared to that of its individual components. Their results also match those observed in earlier studies where CO_2 exhibits a stronger affinity for adsorption than CH_4 on the kerogen components and confined fluids are predominantly in adsorbed state rather than as free gases. In the same vein, Huang et al. [67] studied the fluid states (adsorbed, dissolved, and free) of CH_4 and CO_2 in a confined wet shale environment using an organic-inorganic nanocomposite consisting of Na-montmorillonite sheets and Type I-A kerogen clusters made up of three kerogen molecules. Through hybrid GCMC-MD simulations at 338 K, they quantitatively determined the dynamic distributions of the fluid states of CH_4 and CO_2 during a three-stage shale gas recovery process (initial pressure depletion from 200 to 96 atm, subsequent CO_2 injection at 113 atm, and final pressure depletion from 113 to 96 atm) whilst permitting structure relaxation of the nanocomposite. They uncovered the trend that pressure depletion stages produce mainly free CH_4 whereas CO_2 injection mostly displaces the CH_4 adsorbed within the kerogen. Zhang et al. [68] investigated the competitive adsorption of CO_2 and CH_4 in both silicalite-1 (zeolite) and Type II-D kerogen (organic matter) using GCMC simulations between 300 and 425 K and fluid pressures up to 45 MPa. They showed that both adsorbents exhibit high affinity towards CO_2, with kerogen showing the largest preference for CO_2 and the highest CO_2/CH_4 selectivity. In a follow up study [69], they reported that the adsorption of CH_4 and CO_2 becomes less favourable in the presence of water, however, the strong interactions between CO_2 and kerogen allow the CH_4/CO_2 replacement process to proceed. Using graphite and a model Type II-D kerogen matrix, Li et al. [70,71] utilised GCMC simulations to probe the adsorption behaviours of pure CH_4 and binary mixture of CH_4/CO_2 in environments with varying salinity (up to 6 mol/L NaCl), moisture content (up to 5 wt. % H_2O) and ethane (up to 5 wt. % C_2H_6). They noted that the presence of other compounds inhibits the adsorption of CH_4, with the greatest inhibition at the highest C_2H_6 concentration. Despite the negative impacts on CH_4 loading, the presence of said compounds improves the CO_2/CH_4 selectivity, which could facilitate EGR. More recently, Zhou et al. [72] presented the wettability transition mechanisms on the surface of model Type II-D kerogen (low oxygen content) through 5 ns long MD simulations in NVT ensemble and the supporting DFT calculations. They outlined that at low CO_2 pressures, the kerogen surface is likely to be water-wet and the transition into CO_2-wet state occurs at high CO_2 pressures, hindering capillary trapping of CO_2, which makes CO_2-EGR favourable. Fig. 1.

Overall, these studies offer valuable insights into the adsorption process as well as the CO_2 for CH_4 gas displacement to a certain degree. However, they do not offer a detailed picture describing the CH_4 displacement mechanisms during the CO_2 injection process. Stochastic non-physical moves are sampled during GCMC simulations, such as

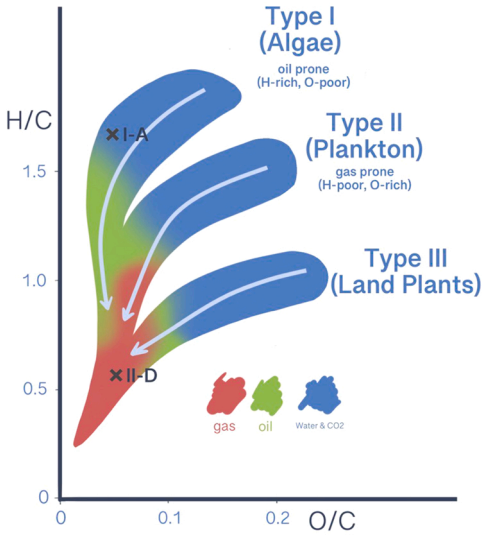

Fig. 1. van Krevelen diagram [73]. The crosses mark the kerogen types investigated in this work. Adapted with permission from Yu et al. [64]. Copyright 2022 American Chemical Society.

particle deletion and reinsertion. While these enable equilibrium to be reached quickly at a given bulk chemical potential, they do not allow the system to evolve over time, meaning that time-dependent properties such as diffusion and displacement/replacement kinetics cannot be quantified. Furthermore, some of the MD studies that do capture time-dependent behaviour suffer from a short simulation time that may not represent the equilibrium state of the system. We recently investigated CH_4 adsorption and diffusion in kerogens of different types and maturity levels using GCMC and equilibrium MD methods [64]. The results show that each individual kerogen matrix exhibits unique physical characteristics such as CH_4 loading, pore size distribution, and helium accessible volume. In addition, this work shows that CH_4 diffuses faster in both immature Type I-A (high H/C ratio) and overmature Type II-D (low H/C ratio) kerogens as compared to the other kerogen types.

In this study, we set out to gain a better understanding of the mechanisms and kinetics of in-situ replacement of CH_4 by CO_2 in model kerogen systems using a constant chemical potential molecular dynamics (CμMD) approach. CμMD works by employing self-adjusting bi-directional bias forces to control the chemical potential of fluids in designated volumes. This way non-equilibrium modelling of concentration-driven processes can be carried out. The CμMD method was first demonstrated to study crystal growth/dissolution at constant solution concentration [74,75]. Then it was extended to research gas transport and separation in porous membranes. This was achieved by maintaining two control volumes of different fluid concentrations at the feed and permeate sides, thereby creating a concentration gradient across a membrane that facilitates the diffusion of molecules [76,77]. Using CμMD, Loganathan and co-workers [78] showcased adsorption of CH_4 and CO_2 onto the surfaces of Na-montmorillonite when exposed to fluids external to the slit-pore at constant reservoir composition. In this work, we used the CμMD technique to understand the recovery mechanisms of CH_4 from organic matter (kerogen) when it is injected with supercritical CO_2. In the CμMD simulations, kerogen slabs pre-adsorbed with CH_4 were exposed to supercritical CO_2. This allowed adsorption kinetics of CO_2 and the consequent desorption of CH_4 to be quantified at constant thermodynamic driving force. In addition, we also provided a contrast between the recovery rate of CH_4 in both immature (Type I-A) and overmature (Type II-D) kerogens (see Fig. 1) by mimicking the real ERG process via CO_2 injection.

2. Methods

2.1. Construction of kerogen slabs

The kerogen slabs used in this study were based on bulk kerogen matrices created in our earlier study [64]. Type I-A (M_w = 3805.1 g/mol, ρ = 0.964 g/cm^3) and Type II-D (M_w = 2468.8 $\pm$ 0.004 g/mol, ρ = 1.119 $\pm$ 0.060 g/cm^3) kerogen macromolecules were designed by Ungerer et al. [79] based on Green River Shale and Duvernay Shales, respectively. Firstly, we used three matrix structures for Type I-A and Type II-D kerogens from our previous study. Then, we loaded the structures with CH_4 based on estimates from earlier GCMC simulations through the RASPA molecular simulation package [80]. In order to create the kerogen slabs, we first replicated the CH_4-loaded kerogen matrices two times in the z-direction, such that the resulting slabs were roughly 10 nm thick in the z-direction, while retaining their x and y dimensions. The kerogen slabs were then centred in a simulation box 30 nm-long in the z-direction, while maintaining the other directions to the same x and y-dimensions as the original kerogen matrices. The remaining void regions of the box were then filled with supercritical CO_2 at density equivalent to 365 K and 275 bar, mimicking reservoir-relevant conditions, at roughly 9.0916 CO_2 molecules per nm^3. Fig. 2 shows the initial configuration of CH_4–CO_2 kerogen systems.

2.2. Simulation settings

All MD simulations were performed using GROMACS 2020.4 molecular dynamics simulation software [81], which was patched with a modified PLUMED version 2.7.1 [82,83] to enable CμMD within the NVT ensemble. Newton's equations of motion were integrated with a time step of 1 fs via the leapfrog algorithm. To control the system temperature, Nosé–Hoover thermostat [84,85] with a coupling time of 0.5 ps was used. The interatomic potentials for the flexible kerogen slabs were obtained from CVFF [86]. The CH_4 and CO_2 molecules were represented by the TraPPE-UA [87] and EPM2-based [88] models, respectively. Short-range non-bonded interactions were described through Lennard–Jones (LJ) potentials. Lorentz-Berthelot mixing rules were used to calculate the LJ interactions of unlike atom pairs in different kerogen macromolecules or further than three bonds of the same macromolecule. Long ranged Coulombic interactions were calculated using a smooth particle mesh Ewald (PME) method [89] of a fourth order polynomial with a mesh width of 0.12 nm. In all simulations, periodic boundary conditions were imposed in all three directions. A cut-off radius of 1.4 nm was used for both the LJ interactions and the real part of the Ewald summation. Dispersion corrections for long range van der Waals interactions were not applied to energy or pressure. The width of the transition regions, control regions, and bias force regions, which are shown in Fig. 2, were set to 2.5, 2.5 and 0.25 nm, respectively. The target density of CO_2 in the control regions was set to reproduce the density of CO_2 at 365 K and 275 bar. The target density of CO_2 in the control regions were maintained by using the force constants, $F_L = F_R$ = 10,000 kJ nm^3 mol^{-1}, which were applied at the centre of the bias force regions (Fig. 2). The concentration of CO_2 in the control regions were monitored over the course of the simulations at intervals of 0.5 ps to ensure the density of CO_2 remains close to the target value. To prevent any shift of the kerogen slabs, we defined a freeze region of 0.5 nm thick in the middle of the simulation box, in which the motion of the kerogen atoms were frozen in the z-direction only. All simulations were carried out at 365 K and for 200 ns in the case of Type I-A and 400 ns for Type II-D kerogen systems. Sample input files, including force field parameters and initial configurations, are available as supplemental material to this article. Details on how to incorporate the CμMD method within PLUMED is available on GitHub (see https://github.com/mme-ucl/CmuMD).

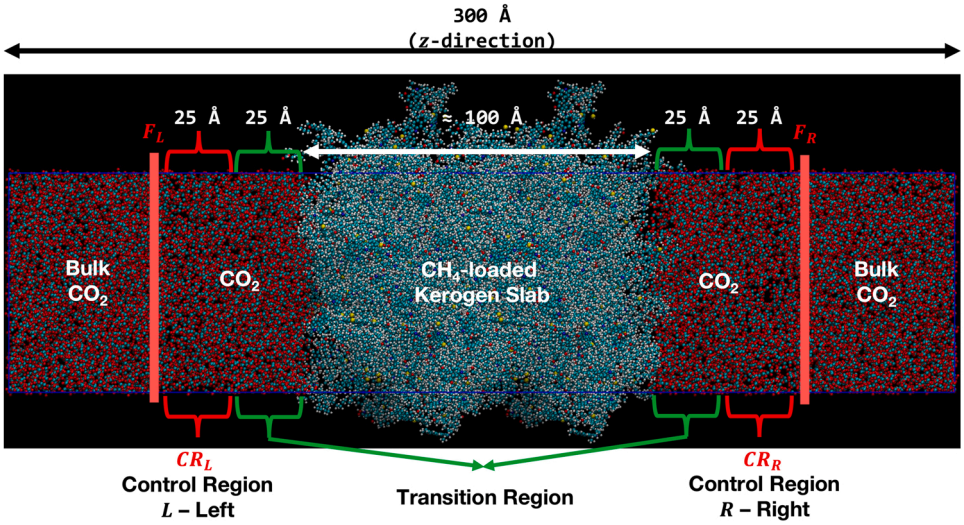

Fig. 2. The initial configuration of the CH_4–CO_2 kerogen systems, where external forces (F_L and F_R) were applied on both sides to maintain constant chemical potential in the control regions (CR_L and CR_R).

2.3. Adsorption/desorption kinetics and diffusion of CH_4 and CO_2 in kerogen

Adsorption is a three-step process, which first involves two mass transport steps external to the adsorption surface (film diffusion and subsequently intraparticle diffusion) and finally surface reaction on the internal surface of the adsorbent. The adsorption rate is the sum of all three steps [90]. Classical kinetics models, namely, pseudo-first order (PFO) and pseudo-second order (PSO) were used to fit the uptake and desorption profiles of CO_2 and CH_4, respectively [91,92]. The linearised forms of the models were provided in Ho and McKay's work [93]. A linear fit can be obtained by plotting $\ln\frac{Q_e}{Q_e-Q(t)}$ vs t and $\frac{t}{Q(t)}$ vs t for PFO and PSO, respectively, where $Q(t)$ is the adsorbate adsorbed at given time, t, or at equilibrium, Q_e. The rate coefficient, k, and equilibrium loading, Q_e, can then be estimated through the slope and intercept of the line of best fit. There is very little consensus regarding the validity of the PFO model, some [94,95] argued it is valid at the initial stage, where the initial concentration is high, while others [96,97] at the final stage of adsorption (near equilibrium). In the case of the PSO model, its superiority compared to the PFO model and wide applicability during adsorption has been reported in the literature [90]. In this study, we compared both the PFO and the PSO models to assess the quality of the fits through the coefficient of determination,R^2, and estimated the adsorption kinetics and/or equilibrium loading amount of CH_4 and CO_2 in Type I-A and Type II-D kerogens.

Gas transport in shale primarily occurs through diffusion, which influences gas recovery as well as the kinetics of the recovery process [27]. In order to improve our understanding of gas transport, we calculated the mean square displacement (MSD) of adsorbed CO_2 in both Type I-A and Type II-D kerogens in the last 50 ns of the simulations. Moreover, the MSD for inaccessible and recovered CH_4 were calculated at the initial (50–100 ns) and final (last 50 ns) stages for Type II-D kerogen systems. The final frames of each simulation were analysed, only CO_2 molecules that have penetrated deeper than 10 Å from the outermost atoms belonging to the kerogen slab at both ends are considered to be in an adsorbed state. In the same way, any remaining CH_4 molecules in Type II-D kerogens are deemed to be in isolated pores or otherwise recovered.

3. Results and discussion

3.1. Kerogen swelling

An earlier study by Pathak et al. [58] suggested that CH_4 replacement with an insufficient amount of CO_2 may lead to kerogen deformation. To assess sorption induced volumetric strain upon CH_4 displacement, Fig. 3 compares the z-density profiles of kerogen slabs before and after simulation in various runs. The z-density profiles of Type I-A and Type II-D kerogen show that Type I-A swells in the z direction more than Type II-D as CH_4 is displaced by CO_2. Initially, the CH_4-loaded Type I-A kerogen slabs have smooth density profiles, whereas the density profiles of CH_4-loaded Type II-D kerogen slabs show large fluctuations indicative of a less homogenous structure in Type II-D (Fig. 3, orange lines). Swelling in the z-direction is observed in the width of the density profile for both kerogen types after CO_2 adsorption and CH_4 desorption (Fig. 3, green lines). The swelling is more significant in Type I-A kerogen, and is reflected in both the density and the slab width. Comparing the density profiles of CH_4 and CO_2 in the z-direction in Type I-A and Type II-D kerogens shows that the CH_4 density in the kerogen slabs decreases over time while the CO_2 density increases (Figs. S1 and S2). The final density profiles for CO_2 in Type I-A kerogen slabs appear similar and have final CO_2 densities that fluctuate around 5 CO_2 molecules/nm^3. The huge variations in density across the z-direction for Type II-D kerogens highlight the structural heterogeneity, which could arise from the preferential parallel stacking arrangement of Type-D kerogen macromolecules [98]. We also observe that, up on CO_2 adsorption, Type II-D kerogens retain more CH_4 than that of Type I-A, suggesting that CO_2 either cannot access or cannot effectively compete with CH_4 for some adsorption sites in the kerogen structures.

3.2. CH_4 recovery in kerogen through supercritical CO_2 exposure

Fig. 4 shows the evolution of CO_2 and CH_4 loadings in Type I-A and Type II-D kerogens as a function of the simulation time. In general, CO_2 is adsorbed more quickly than the CH_4 is desorbed, with the system attaining equilibrium in approx. 100 and 150 ns for Type I-A and Type II-D kerogens, respectively. Looking at Fig. 4, it is apparent that there are two distinct stages for CO_2 uptake, an initial rapid increase and followed by a more gradual uptake before reaching a plateau. Together, the data

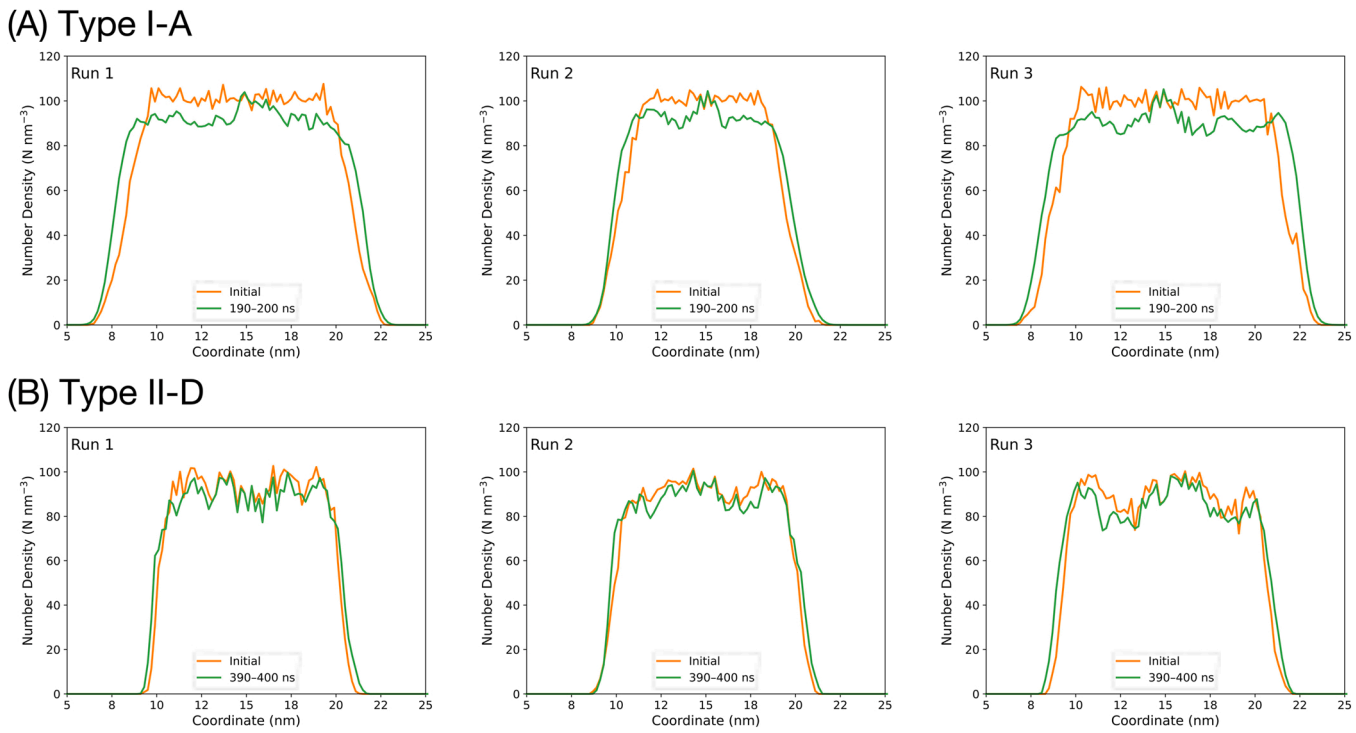

Fig. 3. Density profiles (z-direction) of kerogen slabs in various simulation runs for a) Type I-A and b) Type II-D kerogens.

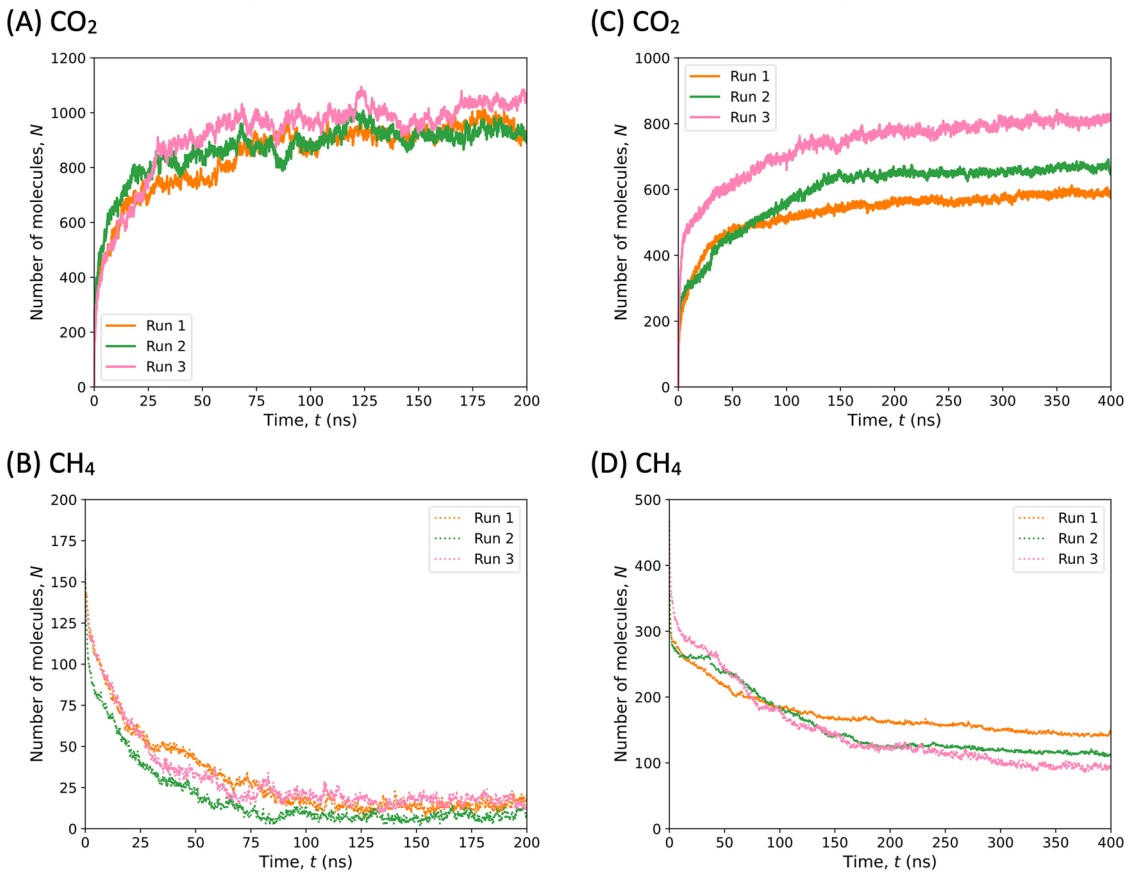

Fig. 4. Methane and carbon dioxide loadings as a function of simulation time in various kerogen slab samples.

suggest that the kinetics of CO_2 adsorption is faster in Type I-A than in Type II-D kerogen. Indeed, MSDs of adsorbed CO_2 molecules in Type I-A and Type II-D computed in the last 50 ns of the simulations show that CO_2 diffuses two to three orders of magnitude faster in Type I-A kerogens compared to that of in Type II-D kerogens (Fig. 5). This suggests that in Type I-A kerogens pores are better connected compared to in Type II-D kerogens. In the case of CH_4 desorption, there is a gradual continuous decrease in CH_4 loading over time, which asymptotically approaches a very low equilibrium loading. Indeed, when the number of CH_4 molecules that remain in Type I-D and Type II-D kerogens at the end of the simulations are compared against the initial number of CH_4 molecules, one can see that in Type I-A kerogen, almost all CH_4 molecules are replaced by the adsorbed CO_2 molecules; whereas, in Type II-D kerogen a significant fraction of the CH_4 molecules still remain adsorbed. This clearly indicates that in Type II-D kerogens, there are CH_4 molecules in isolated pores that are inaccessible to diffusing CO_2 molecules.

Table 1 provides a summary of CH_4 recovery when the kerogen slabs of different maturity levels were exposed to supercritical CO_2. While both kerogens take up more CO_2 molecules than the methane molecules they release, Type I-A kerogen takes up much more CO_2 per initially adsorbed methane than Type II-D. We observe that the inaccessible CH_4 molecules; i.e, those not replaced by CO_2, in Type II-D are an order of magnitude more than the same in Type I-A kerogen. According to the date in Table 1, one CH_4 molecule was replaced by two CO_2 molecules in Type II-D kerogen, whereas in Type I-A kerogens, the replacement ratio is approximately six CO_2 molecules for one CH_4 molecule. Further analysis also shows that CO_2 is most effective at recovering CH_4 in Type I-A with a recovery factor of at least 90 %. For Type II-D kerogen, the recovery factor is in between 65 % and 83 %.

3.3. Kinetics of CH_4 recovery

Figs. S3 and S4 show that the PSO model is a good fit to the CO_2 and CH_4 adsorption/desorption kinetics in Type I-A and Type II-D kerogens, with the fit parameters provided in Table 2. The data show that the equilibrium loadings of CH_4 and CO_2 predicted via the PSO model (Table 2) are in agreement with the average number of CH_4 and CO_2 molecules that are in the kerogen slabs in the last 5 ns of the simulations (Table 1). At first glance, the rate constants show that the CH_4 displacement rate is higher than the adsorption rate of CO_2 in both systems. Closer inspection shows that the rate constants for CH_4 desorption in Type I-A systems are two orders of magnitude higher than in Type II-D. A possible explanation for this might be that CH_4 diffusion in Type I-A is faster than in Type II-D [64]. One unexpected result was that in Run 2 of Type I-A kerogens, the desorption kinetics of CH_4 occur at a rate about two times larger than other runs. This inconsistency may be due to the random packing procedure we used to prepare the underlying kerogen matrix, where structural heterogeneity may emerge [64]. We also observe that the rate of CH_4 desorption in Type II-D systems is at least 3 times faster than CO_2 adsorption rate. It is widely accepted that CO_2 has a higher affinity towards kerogen than CH_4. The lower adsorption rate of CO_2 when compared to CH_4 suggests that diffusion might play a more important role in setting the overall rate than the actual adsorption process at the surface. It can thus be suggested that the CH_4/CO_2 replacement process could be a diffusion-controlled process. The low statistical noise for Type II-D methane desorption is a result of the comparatively small numbers of residual methane molecules in Type I-A kerogen, leading to large fluctuations in the curve at longer times.

Table 1
Number of CH_4 and CO_2 molecules in the kerogen slabs in various simulation runs and the corresponding CH_4 recovery factor and replacement ratio.

Kerogen	Run	CH_4			CO_2	CH_4 Replacement Ratio
		Initial	Final *	Recovery Factor (%)	Final *	
Type I-A	1	170	15	91.18	958	6.18
	2	170	8	95.29	932	5.75
	3	164	17	89.63	1040	7.07
Type II-D	1	394	142	63.96	588	2.33
	2	426	114	73.24	668	2.14
	3	502	93	81.47	810	1.98

* Averaged over the last 5 ns.

Furthermore, we applied the PFO model to obtain the 1st order rate coefficient (k_1) for CO_2 adsorption in kerogens as shown in Fig. S5. It can be seen from Fig. S5 that the quality of fit for the PFO model are subpar as compared to the PSO model (Fig. S4). Since the R^2 values for the fits were all below 0.5, it can be concluded that the PFO model is not suitable for modelling adsorption kinetics for the systems we investigated. CH_4 displacement being well-fit by a PSO process suggests that the rate limiting step in the displacement mechanism is a bimolecular process, though it is unclear what specific species are involved (eg. two CH_4 molecules vs. one CH_4 and one CO_2).

3.4. Analysis of inaccessible CH_4 in Type II-D kerogen

We earlier mentioned that in Type II-D kerogens a fraction of the CH_4 molecules remain trapped despite being exposed to supercritical CO_2. To provide a contrast between recovered and trapped CH_4 molecules in Type II-D kerogens, we computed their used MSD profiles separately. We did this by assigning different labels to the CH_4 molecules that remain in

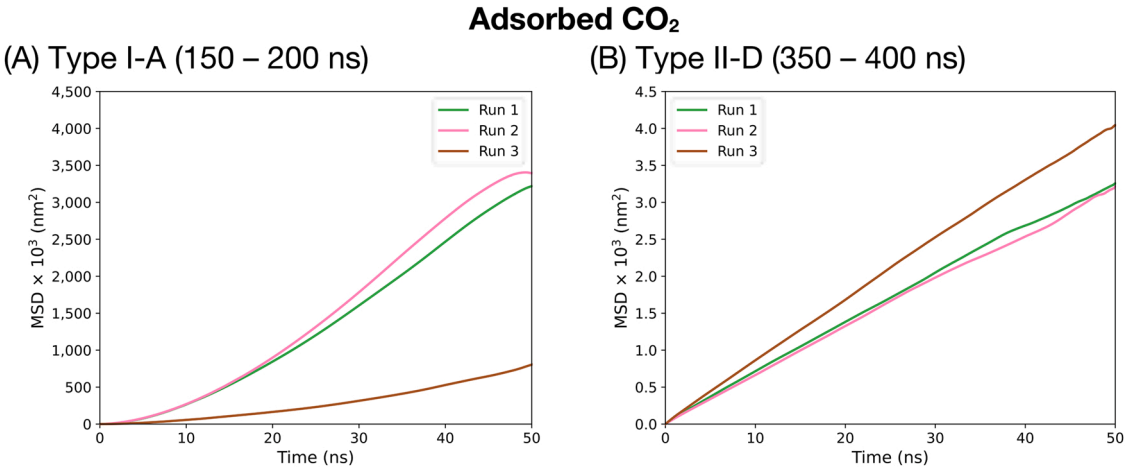

Fig. 5. The MSD plots of adsorbed CO_2 in Type I-A and Type II-D kerogens in the last 50 ns of various simulation runs.

Table 2
Parameters of the linear fit for the PSO kinetic model.

Run	Q_e (mmol/g)*				k_2 (g (mmol ns)$^{-1}$)			
	Type I-A		Type II-D		Type I-A		Type II-D	
	CH_4	CO_2	CH_4	CO_2	CH_4	CO_2	CH_4	CO_2
1	0.0313	2.6317	0.5620	2.4618	-1.4057	0.0351	-0.0816	0.0255
2	0.0160	2.5130	0.4344	2.8573	-3.3487	0.0720	-0.0765	0.0162
3	0.0392	2.8012	0.3550	3.4152	-1.3601	0.0414	-0.0673	0.0172

* To convert no. of mmol of fluid per g kerogen to no. of fluid molecules per kerogen slab, which contains 100 kerogen macromolecules, one needs to multiply the Q_e value by $\frac{M_w}{10}$, where M_w is the molecular weight of the respective kerogen macromolecules.

and outside the kerogen slabs at the end of the simulations; i.e. recovered and residual, respectively. It is worth pointing out that the initially adsorbed CH_4 molecules in Type I-A kerogens were almost completely replaced by CO_2 molecules and hence not included in this analysis. Fig. 6 compares the MSDs of CH_4 molecules in Type II-D kerogen systems. There are two important differences between the recovered and residual CH_4. One, the recovered CH_4 molecules display about an order of magnitude faster diffusion rate as compared to residual CH_4 molecules in the kerogen slabs of Type II-D at any stage of the simulations; and two, at the beginning of the simulations (50–100 ns), where the adsorbed CH_4 content is still high, the MSD of recovered CH_4 is lower than that of recovered CH_4 towards the end of the simulations (350–400 ns), where all recovered CH_4 molecules are outside the kerogen. This is because at the earlier stages, the recovered CH_4 molecules are still in the kerogen matrix where the diffusion is slower compared to that of outside the kerogen. On the other hand, the MSDs of residual CH_4 molecules offer a consistent pattern with no significant differences in magnitude regardless of the progression of the simulations. These observations imply that the residual CH_4 is in a highly constrictive environment, i.e., in narrowly confined pores, thereby inaccessible, and that CO_2 could only displace accessible CH_4 and that inaccessible CH_4 would remain unrecoverable in isolated pores. Comparing the MSDs of both adsorbed CO_2 and trapped CH_4 within Type II-D kerogen slabs, in Figs. 5 and 6, respectively, it is clear that the MSD profiles of the former is higher than that of the latter.

4. Conclusions

In this study, we investigated the kinetics associated with the use of supercritical CO_2 as a means of EGR and GCS through injection in to methane-bearing organic matter, i.e., kerogen. Kerogen in the environment exists at many maturity levels, and it is essential to assess the recovery of CH_4 at the start (immature) and end (overmature) of their lifecycle. This paper offers a comprehensive picture of how kerogen maturity and heterogeneity may impact gas recovery and also the challenges that may arise due to the difference in sorption kinetics. Through CμMD simulations carried out under reservoir-relevant conditions (365 K and 275 bar), this study shows that CO_2 injection can theoretically achieve 90 % and 65 % CH_4 recovery in Type I-A and Type II-D kerogens, respectively. For every CH_4 molecule being replaced, approx. 2–3 and 6–7 CO_2 molecules are being stored in Type II-D and Type I-A kerogens, respectively, where a minute swelling can also be observed during this process. The relatively large number of

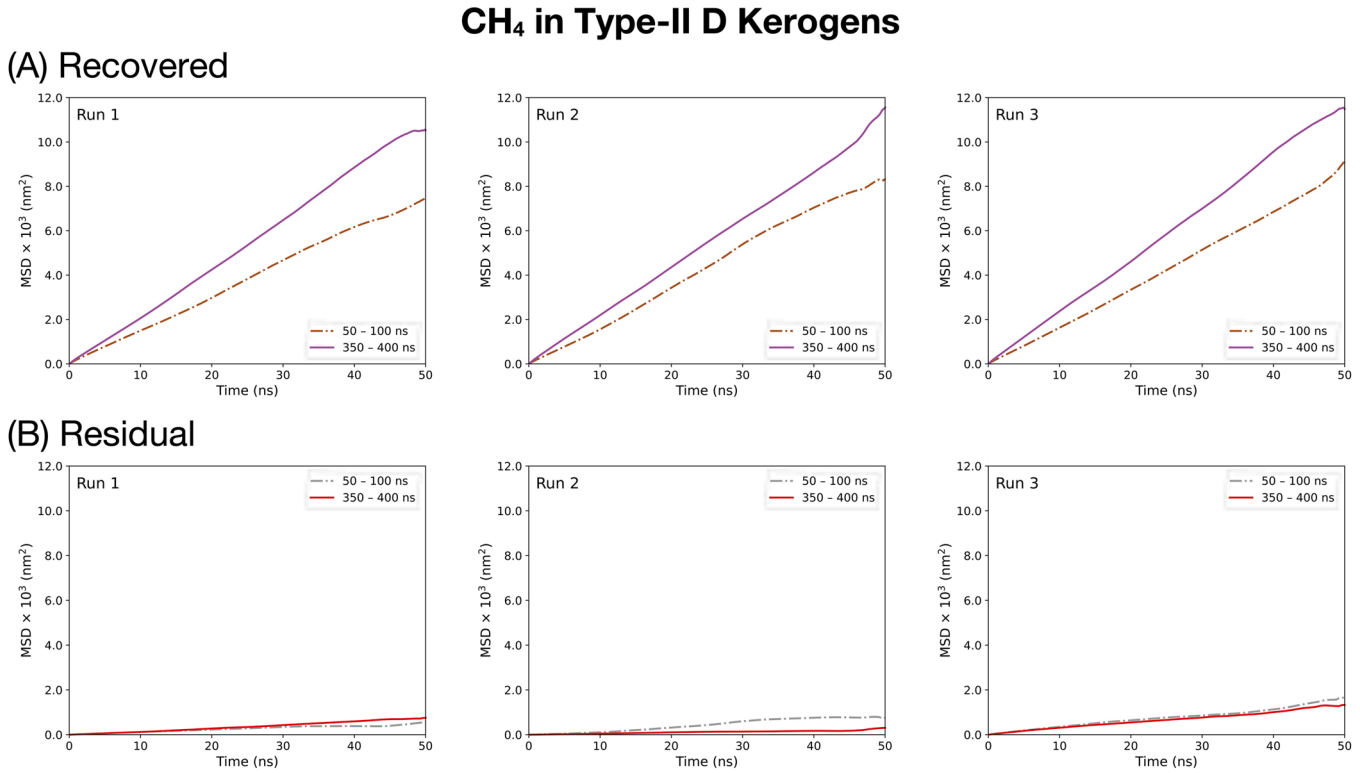

Fig. 6. The MSD plots of recovered and isolated CH_4 in Type II-D kerogen at the initial (50–100 ns) and final (350–400 ns) stages of various simulation runs.

unrecovered CH_4 in Type II-D kerogens is due to the higher density and relatively low pore connectivity of the kerogen slabs, which contain CH_4 in isolated pores that remains trapped within those pores and therefore inaccessible by CO_2. The CO_2 adsorption process is well modelled by a PSO rate law, which is superior to the PFO model at fitting the CO_2 adsorption kinetics. Overall, rapid replacement kinetics can be observed in immature Type I-A kerogens, primarily as a result of fast fluid diffusion through the more porous and flexible slabs, whereas in Type II-D, the kinetics are considerably slower. To the best of our knowledge, this is the first study to quantify the kinetics of the replacement process, i.e., adsorption of CO_2 and the consequent desorption of CH_4, in kerogens. A key strength of this study is the ability to monitor the replacement process in real time while maintaining a constant thermodynamic driving force. The present study lays the groundwork for future molecular level modelling research that can aid improve our understanding of EGR via CO_2 injection into kerogen to achieve net-zero emissions.

CRediT authorship contribution statement

Kai Bin Yu: Data curation, Formal analysis, Methodology, Visualization, Writing – original draft. **Geoffrey M. Bowers:** Conceptualization, Writing – review & editing. **A. Ozgur Yazaydin:** Conceptualization, Methodology, Writing – review & editing, Project administration.

Declaration of Competing Interest

The authors declare that they have no known competing financial interests or personal relationships that could have appeared to influence the work reported in this paper.

Acknowledgements

The authors acknowledge the use of the UCL Myriad High Performance Computing Facility (Myriad@UCL), and associated support services, in the completion of this work. We are grateful to the UK Materials and Molecular Modelling Hub for computational resources, which is partially funded by the Engineering and Physical Sciences Research Council (EP/P020194/1 and EP/T022213/1).

Appendix A. Supporting information

Supplementary data associated with this article can be found in the online version at doi:10.1016/j.jcou.2022.102105.

References

[1] H.R. Zhang, S. Li, K.E. Kelly, E.G. Eddings, Underground in situ coal thermal treatment for synthetic fuels production, Prog. Energy Combust. Sci. 62 (2017) 1–32, https://doi.org/10.1016/j.pecs.2017.05.003.
[2] P. Mahzari, T.M. Mitchell, A.P. Jones, D. Westacott, A. Striolo, Direct gas-in-place measurements prove much higher production potential than expected for shale formations, Sci. Rep. 11 (2021) 10775, https://doi.org/10.1038/s41598-021-90160-3.
[3] U.S. EIA, Technically Recoverable Shale Oil and Shale Gas Resources: An Assessment of 137 Shale Formations in 41 Countries Outside the United States, 2013. ⟨https://www.eia.gov/analysis/studies/worldshalegas/archive/2013/pdf/fullreport_2013.pdf⟩.
[4] R.W. Howarth, R. Santoro, A. Ingraffea, Methane and the greenhouse-gas footprint of natural gas from shale formations, Clim. Change 106 (2011) 679–690, https://doi.org/10.1007/s10584-011-0061-5.
[5] V.A. Kuuskraa, S.H. Stevens, K. Moodhe, Shale Gas Resources: An Assessment of 137 Shale Formations in 41 Countries Outside the United States, Washingt. Indep. Stat. Anal. US Dep. Energy. (2013). ⟨https://www.eia.gov/analysis/studies/worldshalegas/pdf/overview.pdf?zscb=79906188⟩.
[6] A. Striolo, D.R. Cole, Understanding shale gas: recent progress and remaining challenges, Energy Fuels 31 (2017) 10300–10310, https://doi.org/10.1021/acs.energyfuels.7b01023.
[7] Y. Zhang, R. Gautam, S. Pandey, M. Omara, J.D. Maasakkers, P. Sadavarte, D. Lyon, H. Nesser, M.P. Sulprizio, D.J. Varon, R. Zhang, S. Houweling, D. Zavala-Araiza, R. A. Alvarez, A. Lorente, S.P. Hamburg, I. Aben, D.J. Jacob, Quantifying methane emissions from the largest oil-producing basin in the United States from space, Sci. Adv. 6 (2020) eaaz5120, https://doi.org/10.1126/sciadv.aaz5120.
[8] U.S. EPA, Hydraulic Fracturing for Oil and Gas: Impacts from the Hydraulic Fracturing Water Cycle on Drinking Water Resources in the United States. Executive Summary, U.S. Environmental Protection Agency, Washington, DC, EPA/600/R-16/236ES, 2016.
[9] K. Konschnik, A. Dayalu, Hydraulic fracturing chemicals reporting: analysis of available data and recommendations for policymakers, Energy Policy 88 (2016) 504–514, https://doi.org/10.1016/j.enpol.2015.11.002.
[10] E.G. Elliott, A.S. Ettinger, B.P. Leaderer, M.B. Bracken, N.C. Deziel, A systematic evaluation of chemicals in hydraulic-fracturing fluids and wastewater for reproductive and developmental toxicity, J. Expo. Sci. Environ. Epidemiol. 27 (2017) 90–99, https://doi.org/10.1038/jes.2015.81.
[11] Y. Yao, T. Chen, S.S. Shen, Y. Niu, T.L. DesMarais, R. Linn, E. Saunders, Z. Fan, P. Lioy, T. Kluz, L.C. Chen, Z. Wu, M. Costa, Malignant human cell transformation of Marcellus Shale gas drilling flow back water, Toxicol. Appl. Pharmacol. 288 (2015) 121–130, https://doi.org/10.1016/j.taap.2015.07.011.
[12] A. Hamza, I.A. Hussein, M.J. Al-Marri, M. Mahmoud, R. Shawabkeh, S. Aparicio, CO_2 enhanced gas recovery and sequestration in depleted gas reservoirs: a review, J. Pet. Sci. Eng. 196 (2021), 107685, https://doi.org/10.1016/j.petrol.2020.107685.
[13] M. Bui, C.S. Adjiman, A. Bardow, E.J. Anthony, A. Boston, S. Brown, P.S. Fennell, S. Fuss, A. Galindo, L.A. Hackett, J.P. Hallett, H.J. Herzog, G. Jackson, J. Kemper, S. Krevor, G.C. Maitland, M. Matuszewski, I.S. Metcalfe, C. Petit, G. Puxty, J. Reimer, D.M. Reiner, E.S. Rubin, S.A. Scott, N. Shah, B. Smit, J.P.M. Trusler, P. Webley, J. Wilcox, N. Mac Dowell, Carbon capture and storage (CCS): the way forward, Energy Environ. Sci. 11 (2018) 1062–1176, https://doi.org/10.1039/c7ee02342a.
[14] J. Liu, L. Xie, Y. Yao, Q. Gan, P. Zhao, L. Du, Preliminary study of influence factors and estimation model of the enhanced gas recovery stimulated by carbon dioxide utilization in shale, ACS Sustain. Chem. Eng. 7 (2019) 20114–20125, https://doi.org/10.1021/acssuschemeng.9b06005.
[15] R.S. Middleton, J.W. Carey, R.P. Currier, J.D. Hyman, Q. Kang, S. Karra, J. Jiménez-Martínez, M.L. Porter, H.S. Viswanathan, Shale gas and non-aqueous fracturing fluids: opportunities and challenges for supercritical CO_2, Appl. Energy 147 (2015) 500–509, https://doi.org/10.1016/j.apenergy.2015.03.023.
[16] M. Dong, H. Gong, Q. Sang, X. Zhao, C. Zhu, Review of CO_2-kerogen interaction and its effects on enhanced oil recovery and carbon sequestration in shale oil reservoirs, Resour. Chem. Mater. (2022), https://doi.org/10.1016/j.recm.2022.01.006.
[17] T.H. Kim, J. Cho, K.S. Lee, Evaluation of CO_2 injection in shale gas reservoirs with multi-component transport and geomechanical effects, Appl. Energy 190 (2017) 1195–1206, https://doi.org/10.1016/j.apenergy.2017.01.047.
[18] X. Li, D. Elsworth, Geomechanics of CO_2 enhanced shale gas recovery, J. Nat. Gas. Sci. Eng. 26 (2014) 1607–1619, https://doi.org/10.1016/j.jngse.2014.08.010.
[19] C.M. Oldenburg, K. Pruess, S.M. Benson, Process modeling of CO_2 injection into natural gas reservoirs for carbon sequestration and enhanced gas recovery, Energy Fuels 15 (2001) 293–298, https://doi.org/10.1021/ef000247h.
[20] M. Godec, G. Koperna, R. Petrusak, A. Oudinot, Potential for enhanced gas recovery and CO_2 storage in the Marcellus Shale in the Eastern United States, Int. J. Coal Geol. 118 (2013) 95–104, https://doi.org/10.1016/j.coal.2013.05.007.
[21] A.T. Lillies, Sand fracturing with liquid carbon dioxide, Annu. Tech. Meet. ATM 1982 (1982) 6–9, https://doi.org/10.2118/82-33-23.
[22] T. Delschen, A. Hembrock-Heger, U. Necker, Benefits of creating a cross-country data framework for energy efficiency, Lawrence Berkeley National Lab.(LBNL), Berkeley, CA (United States), 1996. ⟨https://www.osti.gov/etdeweb/servlets/purl/22151718⟩.
[23] T. Iiyama, K. Nishikawa, T. Suzuki, K. Kaneko, Study of the structure of a water molecular assembly in a hydrophobic nanospace at low temperature with in situ X-ray diffraction, Chem. Phys. Lett. 274 (1997) 152–158, https://doi.org/10.1016/S0009-2614(97)00664-7.
[24] J. Han, A.K. Bogomolov, E.Y. Makarova, Z. Yang, Y. Lu, X. Li, Molecular simulations on adsorption and diffusion of CO_2 and CH4 in moisture coals, Energy Fuels 31 (2017) 13528–13535, https://doi.org/10.1021/acs.energyfuels.7b02898.
[25] M. Godec, G. Koperna, R. Petrusak, A. Oudinot, Enhanced gas recovery and CO_2 storage in gas shales: a summary review of its status and potential, Energy Procedia 63 (2014) 5849–5857, https://doi.org/10.1016/j.egypro.2014.11.618.
[26] Z. Jin, A. Firoozabadi, Thermodynamic modeling of phase behavior in Shale media, SPE J. 21 (2016) 190–207, https://doi.org/10.2118/176015-PA.
[27] S.R. Etminan, F. Javadpour, B.B. Maini, Z. Chen, Measurement of gas storage processes in shale and of the molecular diffusion coefficient in kerogen, Int. J. Coal Geol. 123 (2014) 10–19, https://doi.org/10.1016/j.coal.2013.10.007.
[28] L. Michalec, M. Lísal, Molecular simulation of shale gas adsorption onto overmature type II model kerogen with control microporosity, Mol. Phys. 115 (2017) 1086–1103, https://doi.org/10.1080/00268976.2016.1243739.
[29] D.G. Hill, C.R. Nelson, Gas productive fractured shales: an overview and update, Gas. TIPS 6 (2000) 4–13.
[30] John B. Curtis, Fractured shale-gas systems, Am. Assoc. Pet. Geol. Bull. 86 (2002) 1921–1938, https://doi.org/10.1306/61eeddbe-173e-11d7-8645000102c1865d.
[31] F. Chen, S. Lu, X. Ding, Y. Ju, Evaluation of the density and thickness of adsorbed methane in differently sized pores contributed by various components in a shale gas reservoir: a case study of the Longmaxi Shale in Southeast Chongqing, China, Chem. Eng. J. 367 (2019) 123–138, https://doi.org/10.1016/j.cej.2019.02.105.
[32] D. Chai, G. Yang, Z. Fan, X. Li, Gas transport in shale matrix coupling multilayer adsorption and pore confinement effect, Chem. Eng. J. 370 (2019) 1534–1549, https://doi.org/10.1016/j.cej.2019.03.276.

[33] P. Chareonsuppanimit, S.A. Mohammad, R.L. Robinson, K.A.M. Gasem, High-pressure adsorption of gases on shales: measurements and modeling, Int. J. Coal Geol. 95 (2012) 34–46, https://doi.org/10.1016/j.coal.2012.02.005.

[34] Z. Sun, X. Li, W. Liu, T. Zhang, M. He, H. Nasrabadi, Molecular dynamics of methane flow behavior through realistic organic nanopores under geologic shale condition: pore size and kerogen types, Chem. Eng. J. 398 (2020), 124341, https://doi.org/10.1016/j.cej.2020.124341.

[35] T. Zhang, G.S. Ellis, S.C. Ruppel, K. Milliken, R. Yang, Effect of organic-matter type and thermal maturity on methane adsorption in shale-gas systems, Org. Geochem. 47 (2012) 120–131, https://doi.org/10.1016/j.orggeochem.2012.03.012.

[36] B.P. Tissot, D.H. Welte, Petroleum formation and occurrence, Springe Berl. Heidelb. Berl. Heidelb. (1984), https://doi.org/10.1007/978-3-642-87813-8.

[37] L. Huang, Z. Ning, Q. Wang, R. Qi, Y. Zeng, H. Qin, H. Ye, W. Zhang, Molecular simulation of adsorption behaviors of methane, carbon dioxide and their mixtures on kerogen: Effect of kerogen maturity and moisture content, Fuel 211 (2018) 159–172, https://doi.org/10.1016/j.fuel.2017.09.060.

[38] L. Huang, Z. Ning, Q. Wang, H. Ye, Z. Chen, Z. Sun, F. Sun, H. Qin, Enhanced gas recovery by CO_2 sequestration in marine shale: a molecular view based on realistic kerogen model, Arab. J. Geosci. 11 (2018) 1–9, https://doi.org/10.1007/s12517-018-3762-5.

[39] J. Li, Y. Wang, Z. Chen, S.S. Rahman, Simulation of adsorption–desorption behavior in coal seam gas reservoirs at the molecular level: a comprehensive review, Energy Fuels 34 (2020) 2619–2642, https://doi.org/10.1021/acs.energyfuels.9b02815.

[40] H. Sun, H. Zhao, N. Qi, Y. Li, Molecular insights into the enhanced shale gas recovery by carbon dioxide in kerogen slit nanopores, J. Phys. Chem. C 121 (2017) 10233–10241, https://doi.org/10.1021/acs.jpcc.7b02618.

[41] K. Mosher, J. He, Y. Liu, E. Rupp, J. Wilcox, Molecular simulation of methane adsorption in micro- and mesoporous carbons with applications to coal and gas shale systems, Int. J. Coal Geol. . 109–110 (2013) 36–44, https://doi.org/10.1016/j.coal.2013.01.001.

[42] R. Heller, M. Zoback, Adsorption of methane and carbon dioxide on gas shale and pure mineral samples, J. Unconv. Oil Gas. Resour. 8 (2014) 14–24, https://doi.org/10.1016/j.juogr.2014.06.001.

[43] L. Huang, Z. Ning, Q. Wang, W. Zhang, Z. Cheng, X. Wu, H. Qin, Effect of organic type and moisture on CO_2/CH4 competitive adsorption in kerogen with implications for CO_2 sequestration and enhanced CH4 recovery, Appl. Energy 210 (2018) 28–43, https://doi.org/10.1016/j.apenergy.2017.10.122.

[44] P. Charoensuppanimit, S.A. Mohammad, K.A.M. Gasem, Measurements and modeling of gas adsorption on shales, Energy Fuels. 30 (2016) 2309–2319, https://doi.org/10.1021/acs.energyfuels.5b02751.

[45] H. Zhao, T. Wu, A. Firoozabadi, High pressure sorption of various hydrocarbons and carbon dioxide in Kimmeridge Blackstone and isolated kerogen, Fuel 224 (2018) 412–423, https://doi.org/10.1016/j.fuel.2018.02.186.

[46] S. Sanguinito, A. Goodman, M. Tkach, B. Kutchko, J. Culp, S. Natesakhawat, J. Fazio, I. Fukai, D. Crandall, Quantifying dry supercritical CO_2-induced changes of the Utica Shale, Fuel 226 (2018) 54–64, https://doi.org/10.1016/j.fuel.2018.03.156.

[47] T. Wu, H. Zhao, S. Tesson, A. Firoozabadi, Absolute adsorption of light hydrocarbons and carbon dioxide in shale rock and isolated kerogen, Fuel 235 (2019) 855–867, https://doi.org/10.1016/j.fuel.2018.08.023.

[48] H. Zhao, Z. Lai, A. Firoozabadi, Sorption hysteresis of light hydrocarbons and carbon dioxide in shale and kerogen, Sci. Rep. 7 (2017) 16209, https://doi.org/10.1038/s41598-017-13123-7.

[49] A. Gonciaruk, M.R. Hall, M.W. Fay, C.D.J. Parmenter, C.H. Vane, A.N. Khlobystov, N. Ripepi, Kerogen nanoscale structure and CO_2 adsorption in shale micropores, Sci. Rep. 11 (2021) 1–13, https://doi.org/10.1038/s41598-021-83179-z.

[50] S. Wang, X. Yao, Q. Feng, F. Javadpour, Y. Yang, Q. Xue, X. Li, Molecular insights into carbon dioxide enhanced multi-component shale gas recovery and its sequestration in realistic kerogen, Chem. Eng. J. 425 (2021), 130292, https://doi.org/10.1016/j.cej.2021.130292.

[51] R. Khosrokhavar, K.H. Wolf, H. Bruining, Sorption of CH4 and CO_2 on a carboniferous shale from Belgium using a manometric setup, Int. J. Coal Geol. 128–129 (2014) 153–161, https://doi.org/10.1016/j.coal.2014.04.014.

[52] T. Wang, S. Tian, G. Li, L. Zhang, M. Sheng, W. Ren, Molecular simulation of gas adsorption in shale nanopores: a critical review, Renew. Sustain. Energy Rev. 149 (2021), 111391, https://doi.org/10.1016/j.rser.2021.111391.

[53] H. Sui, J. Yao, Effect of surface chemistry for CH4/CO_2 adsorption in kerogen: a molecular simulation study, J. Nat. Gas. Sci. Eng. 31 (2016) 738–746, https://doi.org/10.1016/j.jngse.2016.03.097.

[54] T. Wang, S. Tian, G. Li, M. Sheng, W. Ren, Q. Liu, S. Zhang, Molecular simulation of CO_2/CH4 competitive adsorption on shale kerogen for CO_2 sequestration and enhanced gas recovery, J. Phys. Chem. C 122 (2018) 17009–17018, https://doi.org/10.1021/acs.jpcc.8b02061.

[55] L. Huang, Z. Ning, Q. Wang, R. Qi, Z. Cheng, X. Wu, W. Zhang, H. Qin, Molecular insights into kerogen deformation induced by CO_2/CH4 sorption: effect of maturity and moisture, Energy Fuels 33 (2019) 4792–4805, https://doi.org/10.1021/acs.energyfuels.9b00409.

[56] M. Kazemi, H. Maleki, A. Takbiri-Borujeni, Molecular dynamics study of transport and storage of methane in kerogen, SPE East. Reg. Meet. 2016-January (2016) 13–15, https://doi.org/10.2118/184058-MS.

[57] M. Vasileiadis, L.D. Peristeras, K.D. Papavasileiou, I.G. Economou, Modeling of bulk kerogen porosity: methods for control and characterization, Energy Fuels 31 (2017) 6004–6018, https://doi.org/10.1021/acs.energyfuels.7b00626.

[58] M. Pathak, H. Huang, P. Meakin, M. Deo, Molecular investigation of the interactions of carbon dioxide and methane with kerogen: application in enhanced shale gas recovery, J. Nat. Gas. Sci. Eng. 51 (2018) 1–8, https://doi.org/10.1016/j.jngse.2017.12.021.

[59] M. Vasileiadis, L.D. Peristeras, K.D. Papavasileiou, I.G. Economou, Transport properties of shale gas in relation to kerogen porosity, J. Phys. Chem. C 122 (2018) 6166–6177, https://doi.org/10.1021/acs.jpcc.8b00162.

[60] T. Wu, A. Firoozabadi, Effect of microstructural flexibility on methane flow in kerogen matrix by molecular dynamics simulations, J. Phys. Chem. C 123 (2019) 10874–10880, https://doi.org/10.1021/acs.jpcc.8b12328.

[61] T.A. Ho, Y. Wang, L.J. Criscenti, Chemo-mechanical coupling in kerogen gas adsorption/desorption, Phys. Chem. Chem. Phys. 20 (2018) 12390–12395, https://doi.org/10.1039/c8cp01068d.

[62] S. Tesson, A. Firoozabadi, Methane adsorption and self-diffusion in shale kerogen and slit nanopores by molecular simulations, J. Phys. Chem. C 122 (2018) 23528–23542, https://doi.org/10.1021/acs.jpcc.8b07123.

[63] Z. Li, J. Yao, A. Firoozabadi, Kerogen swelling in light hydrocarbon gases and liquids and validity of Schroeder's paradox, J. Phys. Chem. C 125 (2021) 8137–8147, https://doi.org/10.1021/acs.jpcc.0c10362.

[64] K. Bin Yu, G.M. Bowers, N. Loganathan, A.G. Kalinichev, A.O. Yazaydin, Diffusion behavior of methane in 3D kerogen models, Energy Fuels. 35 (2021) 16515–16526, https://doi.org/10.1021/acs.energyfuels.1c02167.

[65] J. Collell, G. Galliero, F. Gouth, F. Montel, M. Pujol, P. Ungerer, M. Yiannourakou, Molecular simulation and modelisation of methane/ethane mixtures adsorption onto a microporous molecular model of kerogen under typical reservoir conditions, Microporous Mesoporous Mater. 197 (2014) 194–203, https://doi.org/10.1016/j.micromeso.2014.06.016.

[66] K. Adewumi Babatunde, B. Mamo Negash, M. Rashik Mojid, T.Y. Ahmed, S. Regassa Jufar, Molecular simulation study of CO_2/CH4 adsorption on realistic heterogeneous shale surfaces, Appl. Surf. Sci. 543 (2021), 148789, https://doi.org/10.1016/j.apsusc.2020.148789.

[67] L. Huang, W. Zhou, H. Xu, L. Wang, J. Zou, Q. Zhou, Dynamic fluid states in organic-inorganic nanocomposite: implications for shale gas recovery and CO_2 sequestration, Chem. Eng. J. 411 (2021), 128423, https://doi.org/10.1016/j.cej.2021.128423.

[68] K. Zhang, H. Jiang, G. Qin, Utilization of zeolite as a potential multi-functional proppant for CO_2 enhanced shale gas recovery and CO_2 sequestration: a molecular simulation study on the competitive adsorption of CH4 and CO_2 in zeolite and organic matter, Fuel 249 (2019) 119–129, https://doi.org/10.1016/j.fuel.2019.03.061.

[69] K. Zhang, H. Jiang, G. Qin, Utilization of zeolite as a potential multi-functional proppant for CO_2 enhanced shale gas recovery and CO_2 sequestration: a molecular simulation study of the impact of water on adsorption in zeolite and organic matter, Fuel 292 (2021), 120312, https://doi.org/10.1016/j.fuel.2021.120312.

[70] J. Li, Y. Wang, Z. Chen, S.S. Rahman, Effects of moisture, salinity and ethane on the competitive adsorption mechanisms of CH4/CO_2 with applications to coalbed reservoirs: a molecular simulation study, J. Nat. Gas. Sci. Eng. 95 (2021), 104151, https://doi.org/10.1016/j.jngse.2021.104151.

[71] J. Li, Y. Wang, Z. Chen, S.S. Rahman, Insights into the molecular competitive adsorption mechanism of CH4/CO2in a kerogen matrix in the presence of moisture, salinity, and ethane, Langmuir 37 (2021) 12732–12745, https://doi.org/10.1021/acs.langmuir.1c02274.

[72] J. Zhou, J. Zhang, J. Yang, Z. Jin, K.H. Luo, Mechanisms for kerogen wettability transition from water-wet to CO_2-wet: implications for CO_2 sequestration, Chem. Eng. J. 428 (2022), 132020, https://doi.org/10.1016/j.cej.2021.132020.

[73] D.W. van Krevelen. Coal: Typology, Physics, Chemistry, Constitution, 3rd ed., Elsevier, Amsterdam, 1993.

[74] T. Karmakar, P.M. Piaggi, C. Perego, M. Parrinello, A Cannibalistic approach to grand canonical crystal growth, J. Chem. Theory Comput. 14 (2018) 2678–2683, https://doi.org/10.1021/acs.jctc.8b00191.

[75] C. Perego, M. Salvalaglio, M. Parrinello, Molecular dynamics simulations of solutions at constant chemical potential, J. Chem. Phys. 142 (2015), https://doi.org/10.1063/1.4917200.

[76] A. Ozcan, R. Semino, G. Maurin, A.O. Yazaydin, Modeling of gas transport through polymer/MOF interfaces: a microsecond-scale concentration gradient-driven molecular dynamics study, Chem. Mater. 32 (2020) 1288–1296, https://doi.org/10.1021/acs.chemmater.9b04907.

[77] A. Ozcan, C. Perego, M. Salvalaglio, M. Parrinello, O. Yazaydin, Concentration gradient driven molecular dynamics: a new method for simulations of membrane permeation and separation, Chem. Sci. 8 (2017) 3858–3865, https://doi.org/10.1039/c6sc04978h.

[78] N. Loganathan, G.M. Bowers, B.F. Ngouana Wakou, A.G. Kalinichev, R. J. Kirkpatrick, A.O. Yazaydin, Understanding methane/carbon dioxide partitioning in clay nano- and meso-pores with constant reservoir composition molecular dynamics modeling, Phys. Chem. Chem. Phys. 21 (2019) 6917–6924, https://doi.org/10.1039/c9cp00851a.

[79] P. Ungerer, J. Collell, M. Yiannourakou, Molecular modeling of the volumetric and thermodynamic properties of kerogen: influence of organic type and maturity, Energy Fuels 29 (2015) 91–105, https://doi.org/10.1021/ef502154k.

[80] D. Dubbeldam, S. Calero, D.E. Ellis, R.Q. Snurr, RASPA: molecular simulation software for adsorption and diffusion in flexible nanoporous materials, Mol. Simul. 42 (2016) 81–101, https://doi.org/10.1080/08927022.2015.1010082.

[81] M.J. Abraham, T. Murtola, R. Schulz, S. Páll, J.C. Smith, B. Hess, E. Lindah, Gromacs: high performance molecular simulations through multi-level parallelism from laptops to supercomputers, Softw. 1–2 (2015) 19–25, https://doi.org/10.1016/j.softx.2015.06.001.

[82] G.A. Tribello, M. Bonomi, D. Branduardi, C. Camilloni, G. Bussi, PLUMED 2: new feathers for an old bird, Comput. Phys. Commun. 185 (2014) 604–613, https://doi.org/10.1016/j.cpc.2013.09.018.
[83] The PLUMED consortium, Promoting transparency and reproducibility in enhanced molecular simulations, Nat. Methods 16 (2019) 670–673, https://doi.org/10.1038/s41592-019-0506-8.
[84] S. Nosé, A molecular dynamics method for simulations in the canonical ensemble, Mol. Phys. 52 (1984) 255–268, https://doi.org/10.1080/00268978400101201.
[85] W.G. Hoover, Canonical dynamics: equilibrium phase-space distributions, Phys. Rev. A 31 (1985) 1695–1697, https://doi.org/10.1103/PhysRevA.31.1695.
[86] A.T. Hagler, S. Lifson, P. Dauber, Consistent force field studies of intermolecular forces in hydrogen-bonded crystals. 2. A benchmark for the objective comparison of alternative force fields, J. Am. Chem. Soc. 101 (1979) 5122–5130, https://doi.org/10.1021/ja00512a002.
[87] M.G. Martin, J.I. Siepmann, Transferable potentials for phase equilibria. 1. United-atom description of n -alkanes, J. Phys. Chem. B 102 (1998) 2569–2577, https://doi.org/10.1021/jp972543.
[88] R.T. Cygan, V.N. Romanov, E.M. Myshakin, Molecular simulation of carbon dioxide capture by montmorillonite using an accurate and flexible force field, J. Phys. Chem. C 116 (2012) 13079–13091, https://doi.org/10.1021/jp3007574.
[89] U. Essmann, L. Perera, M.L. Berkowitz, T. Darden, H. Lee, L.G. Pedersen, A smooth particle mesh Ewald method, J. Chem. Phys. 103 (1995) 8577–8593, https://doi.org/10.1063/1.470117.
[90] K.L. Tan, B.H. Hameed, Insight into the adsorption kinetics models for the removal of contaminants from aqueous solutions, J. Taiwan Inst. Chem. Eng. 74 (2017) 25–48, https://doi.org/10.1016/j.jtice.2017.01.024.
[91] J.P. Simonin, On the comparison of pseudo-first order and pseudo-second order rate laws in the modeling of adsorption kinetics, Chem. Eng. J. 300 (2016) 254–263, https://doi.org/10.1016/j.cej.2016.04.079.
[92] A.L. Ballard, E.D. Sloan, The next generation of hydrate prediction: an overview, J. Supramol. Chem. 2 (2002) 385–392, https://doi.org/10.1016/S1472-7862(03)00063-7.
[93] Y.S. Ho, G. McKay, Pseudo-second order model for sorption processes, Process Biochem 34 (1999) 451–465, https://doi.org/10.1016/S0032-9592(98)00112-5.
[94] G. McKay, Y.S. Ho, J.C.Y. Ng, Biosorption of copper from waste waters: a review, Sep. Purif. Methods 28 (1999) 87–125, https://doi.org/10.1080/03602549909351645.
[95] Y.S. Ho, G. McKay, The sorption of lead(II) ions on peat, Water Res. 33 (1999) 578–584, https://doi.org/10.1016/S0043-1354(98)00207-3.
[96] W. Plazinski, W. Rudzinski, A. Plazinska, Theoretical models of sorption kinetics including a surface reaction mechanism: a review, Adv. Colloid Interface Sci. 152 (2009) 2–13, https://doi.org/10.1016/j.cis.2009.07.009.
[97] W. Rudzinski, W. Plazinski, Studies of the kinetics of solute adsorption at solid/solution interfaces: On the possibility of distinguishing between the diffusional and the surface reaction kinetic models by studying the pseudo-first-order kinetics, J. Phys. Chem. C. 111 (2007) 15100–15110, https://doi.org/10.1021/jp073249c.
[98] E. Rezlerová, J.K. Brennan, M. Lísal, Methane and carbon dioxide in dual-porosity organic matter: molecular simulations of adsorption and diffusion, AIChE J. (2020) 1–17, https://doi.org/10.1002/aic.16655.